ACS APPLIED MATERIALS & INTERFACES

Research Article

www.acsami.org

Nanostructured Porous Si Optical Biosensors: Effect of Thermal Oxidation on Their Performance and Properties

Giorgi Shtenberg,[†] Naama Massad-Ivanir,[‡] Ljiljana Fruk,[§] and Ester Segal*[,‡,∥]

[†]The Inter-Departmental Program of Biotechnology, [‡]Department of Biotechnology and Food Engineering, and [∥]The Russell Berrie Nanotechnology Institute, Technion—Israel Institute of Technology, Haifa 32000, Israel

[§]DFG—Center for Functional Nanostructures, Karlsruhe Institute of Technology, Karlsruhe 76131, Germany

Supporting Information

ABSTRACT: The influence of thermal oxidation conditions on the performance of porous Si optical biosensors used for label-free and real-time monitoring of enzymatic activity is studied. We compare three oxidation temperatures (400, 600, and 800 °C) and their effect on the enzyme immobilization efficiency and the intrinsic stability of the resulting oxidized porous Si ($PSiO_2$), Fabry–Pérot thin films. Importantly, we show that the thermal oxidation profoundly affects the biosensing performance in terms of greater optical sensitivity, by monitoring the catalytic activity of horseradish peroxidase and trypsin-immobilized $PSiO_2$. Despite the significant decrease in porous volume and specific surface area (confirmed by nitrogen gas adsorption–desorption studies) with elevating the oxidation temperature, higher content and surface coverage of the immobilized enzymes is attained. This in turn leads to greater optical stability and sensitivity of $PSiO_2$ nanostructures. Specifically, films produced at 800 °C exhibit stable optical readout in aqueous buffers combined with superior biosensing performance. Thus, by proper control of the oxide layer formation, we can eliminate the aging effect, thus achieving efficient immobilization of different biomolecules, optical signal stability, and sensitivity.

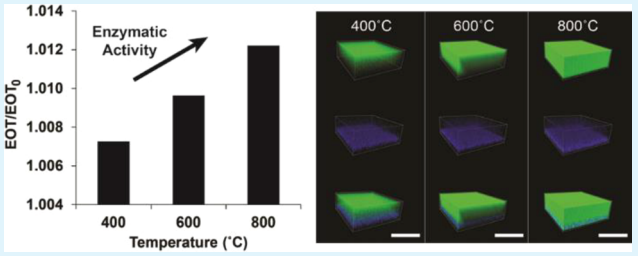

KEYWORDS: *biosensor, enzyme, nanostructure, porous Si, thermal oxidation, label free*

INTRODUCTION

Nanostructured porous Si (PSi) has emerged as an attractive and versatile material for optical biosensing applications due to its large internal surface area and tunable optical properties.[1−5] Various biosensing schemes have shown numerous advantages of these nanosystems over conventional bioanalytical techniques, such as enhanced detection sensitivity, real-time and label-free fast analysis.[1,6−24] However, a critical challenge in designing PSi-based biosensors is the relative chemical instability of the Si scaffold in biologically relevant environments.[25−28] Specifically, PSi can be oxidized and/or dissolved in aqueous environments, which can lead to significant variations in the optical and electrical properties, e.g., luminescence, refractive index, and absorption coefficient.[26,29−31] For example, PSi oxidation can significantly affect the refractive index of the material (n = 3.5 and n = 1.4 for Si and SiO_2, respectively) and thus it can interfere with the signal transduction in PSi optical biosensors. Moreover, PSi dissolution in aqueous media causes an even higher change in the refractive index, which may ultimately result in the structural collapse of the porous matrix.[14,31] Several chemical routes are used to enhance PSi stability in biological media, including thermal oxidation, hydrosilylation, electrochemical alkylation, and thermal hydrocarbonization.[2,31−33] Thermal oxidation is frequently utilized for PSi biosensor passivation, owing to the wide repertoire of chemical modifications available for silicon oxide surfaces. The high temperature treatment completely converts the reactive SiH_x species into relatively inert Si–O bonds, resulting in a greater optical stability, potentially eliminating zero-point drift, and protection against aqueous dissolution.[19,21]

Herewith, we study the effect of thermal oxidation conditions on the stability and sensitivity of PSi-based optical biosensors, which are designed for monitoring enzymatic activity. The effect of different oxidation conditions (temperature) on the chemical stabilization of the biosensor surface, i.e., PSi Fabry–Pérot thin film, is investigated. We demonstrate that, by proper control of the oxide layer formation, the aging effect can be eliminated, thus leading to an efficient bioconjugation of different molecules, optical signal stability, and sensitivity.

EXPERIMENTAL SECTION

Materials. Silicon wafers (highly doped p-type, 0.8 mΩ·cm resistivity, ⟨100⟩ oriented, boron-doped) were supplied by Siltronix Corp. Aqueous HF (48%) and absolute ethanol were obtained from Merck. 3-Aminopropyl(triethoxyl)silane (APTES), diisopropylethylamine (DIEA), bis(*N*-succinimidyl)carbonate (DSC), horseradish peroxidase (HRP) type VI, trypsin from bovine pancreas (treated

Received: June 20, 2014
Accepted: August 27, 2014
Published: August 27, 2014

with L-1-tosylamido-2-phenylethyl chloromethyl ketone, TPCK), acetonitrile, hydrogen peroxide (H_2O_2), Ampliflu Red, 4-chloro-1-naphthol (4CN), and analytical grade buffers were supplied by Sigma-Aldrich Chemicals. Fluorescein thiocarbamoyl labeled casein (FTC-casein) and fluorescein-5-EX, succinimidyl ester, were obtained from Thermo Fisher Scientific Inc.

Preparation of Porous SiO_2 Nanostructures. PSi thin films are prepared by anodization at a current density of 385 mA cm^{-2} as previously described by Massad-Ivanir et al.[6] Then, the PSi samples are thermally oxidized at three temperatures, 400, 600, and 800 °C, for 1 h, resulting in porous SiO_2 ($PSiO_2$) layers.[6]

The following sections describe the biofunctionalization procedures and the consecutive biosensing experiments, which are carried out for the $PSiO_2$ layers, formed at 400, 600, and 800 °C.

Biofunctionalization of $PSiO_2$. *Preparation of APTES-Modified and DSC-Modified Surfaces.* The $PSiO_2$ samples are prepared as previously described by Massad-Ivanir et al.[6]

Preparation of Enzyme-Immobilized Surfaces. The DSC-modified surfaces are incubated with 30 μL of enzyme solution (2.5 μM and 4.6 μM, HRP and trypsin, respectively) in 0.1 M *N*-(2-hydroxyethyl)-piperazine-*N*′-ethanesulfonic acid (HEPES) buffer (pH 8) for 1 h at room temperature. After the removal of solution, the surfaces are washed with HEPES buffer, soaked for 20 min in buffer, and washed with HEPES to exclude the nonspecifically bound enzymes from the surfaces.

Nitrogen Adsorption−Desorption Measurements. The different oxidized (400, 600, and 800 °C) $PSiO_2$ nanostructures are analyzed as previously described.[34] Note that, before the adsorption experiment is conducted, the samples are degassed in situ at 200 °C for 10 h.

Gravimetric Determination of Porosity and Infrared Spectroscopy. Detailed analysis is performed as previously described.[6]

Thermal Gravimetric Analysis (TGA). Thermogravimetric analysis is conducted using a TA Instruments Q5000-0486 TGA. The freshly etched PSi samples are heated between 25 °C and the designated oxidation temperature (400, 600, and 800 °C), under nitrogen atmosphere, at a constant heating rate of 20 °C min^{-1}.

Energy-Dispersive X-ray Spectroscopy (EDS). A Carl Zeiss Ultra Plus high-resolution scanning electron microscope (HRSEM) coupled with an EDS detector is used to determine the oxidation degrees of the different porous nanostructures. EDS elemental mapping is performed at an acceleration voltage of 10 kV using Espirit 1.8 software.

Confocal Laser Scanning Microscopy (CLSM). HRP and trypsin are modified with fluorescein-5-EX, succinimidyl ester, according to the manufacturer's protocol. The labeled enzyme solution in HEPES buffer (at concentrations of 2.5 μM fluorescein-HRP and 4.6 μM fluorescein-trypsin, respectively) is incubated with the DSC-modified $PSiO_2$ for 1 h at room temperature. After the solution is removed, the surfaces are thoroughly washed with HEPES buffer, soaked for 1 h in buffer, and washed again with buffer to exclude any nonspecifically bound enzymes from the surfaces. Following the conjugation, the samples are scanned with a LSM 700 confocal laser scanning microscope (Carl Zeiss, Inc.) connected to a Zeiss inverted microscope equipped with a Zeiss X63 oil immersion objective. Combinations of 405 and 488 nm laser lines are used for the excitation of the $PSiO_2$ structure and FTC-modified enzymes, respectively. For three-dimensional (3D) image projection of the enzyme-immobilized $PSiO_2$, *z*-scans in 0.35 μm increments are taken over a depth of ∼6.6 μm and projected by using standard Carl Zeiss software (ZEN 2009). Image analysis is performed by Imaris Bitplane scientific software.

Enzymatic Activity. *HRP Activity.* Ampliflu Red substrate solutions and HRP activity assay are performed as previously described.[35]

Trypsin Activity. FTC-casein solution (200 μL of 0.38 μM) in a HEPES buffer is introduced onto trypsin-immobilized $PSiO_2$ samples. The catalytic reaction progress is monitored at room temperature by recording the fluorescence values at 538 nm (excitation wavelength of 485 nm).

Quantification of Immobilized Enzyme. The amount of immobilized enzyme is determined by comparing the specific activity rates of various concentrations of the free enzyme in a solution (calibration curves: trypsin and HRP, 2−650 and 20−160 nM, respectively) to the immobilized enzyme activity.

Optical Measurements. Detailed optical characteristics of the $PSiO_2$ film, the system setup, and data analysis are described elsewhere.[6] Briefly, the effective optical thickness (EOT) refers to the $2nL$ term in the Fabry−Pérot formula (where n is the average refractive index and L is the porous layer thickness).[6] In the present work, the data are presented as relative EOT and defined as

$$\frac{\mathrm{EOT}}{\mathrm{EOT}_0} = \left(\frac{\mathrm{EOT}_{\text{chemical modification}}}{\mathrm{EOT}_{\mathrm{PSiO_2}}}\right)_T \quad (1)$$

where $\mathrm{EOT}_{\text{chemical modification}}$ is the value of nL obtained after different biofunctionalization steps (e.g., APTES, DSC, HRP immobilization), $\mathrm{EOT}_{\mathrm{PSiO_2}}$ is the nL_0 value of the neat $PSiO_2$, and T refers to the thermal oxidation temperature.

Optical Readout Stability of $PSiO_2$-Based Transducers. Neat $PSiO_2$, APTES-modified $PSiO_2$, DSC-modified $PSiO_2$, trypsin, and HRP-immobilized $PSiO_2$ are washed with HEPES buffer at a constant flow of 0.5 mL min^{-1} for 260 min. The reflectivity spectra are collected throughout the experiments every 30 s.

Optical Biosensing of HRP Activity. HRP-immobilized $PSiO_2$ surfaces are washed with HEPES buffer for 30 min. Then, 0.8 mM 4CN in HEPES buffer is cycled through a custom-made flow cell for 20 min. Lastly, 0.16 M H_2O_2 is introduced into the cycled solution for enzyme activation. The reflectivity spectra are recorded throughout the experiments every 30 s.[36]

RESULTS AND DISCUSSION

Characterization of $PSiO_2$ Films. The $PSiO_2$ surfaces are prepared using anodic electrochemical etching of heavily doped Si, followed by thermal oxidation in ambient air at three different temperatures (400, 600, and 800 °C) to generate a hydrophilic scaffold.[6] Previous work by Pap et al.[29] has established that thermal oxidation of PSi at 800 °C for a duration of 1 h results in a high conversion (>80%) of the hydrogen-terminated Si to SiO_2. At lower temperatures (400 and 600 °C), extending the oxidation time has a limited effect on the oxidation degree. These results are explained by taking into account the thickness and porosity of the porous nanostructure and the rate of diffusion through the layer. The structural properties of the obtained thermally oxidized porous nanostructures correspond to those previously described by Segal et al.[3] The porous film is 6830 ± 150 nm thick, characterized by cylindrically shaped pores with diameters of 60−100 nm. EDS coupled to HRSEM and TGA are employed in order to characterize the resulting oxide layer and the $PSiO_2$ films. Figure 1a summarizes the elemental analysis results, expressed in terms of relative atomic percentage of oxygen to Si, for the different $PSiO_2$ layers.[37] The oxygen to Si ratio is observed to significantly increase with oxidation temperature, indicative of a thicker and more dense oxide layer,[33] in agreement with TGA data (see Figure S1, Supporting Information). It should be noted that the porous film is highly irregular and rough at the nanoscale and a thicker and denser oxide layer would have a profound effect on the surface homogeneity. Figure 1b−d depicts EDS−HRSEM results for the $PSiO_2$ films oxidized at 800 °C.

Furthermore, attenuated total reflectance Fourier transform infrared (ATR-FTIR) spectroscopy is used as a complementary tool for surface characterization. Figure S2 in the Supporting Information depicts the ATR-FTIR spectra at the different

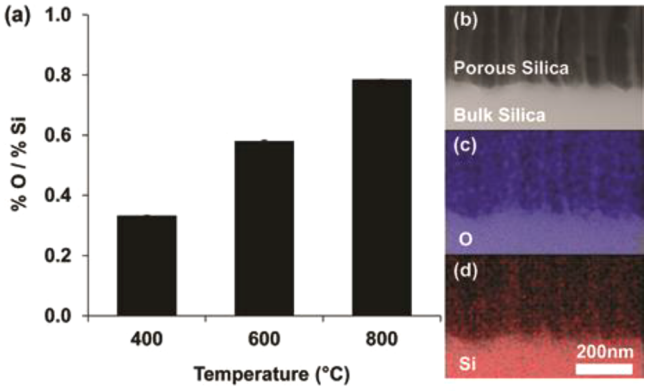

Figure 1. Elemental analysis of PSi nanostructure oxidized at different temperatures. (a) Ratio of atomic percentages, obtained by EDS mapping, of oxide to Si across the porous layer, for films oxidized at different temperatures (400, 600, 800 °C). The error is less than ±0.004. (b) Cross-section HRSEM micrograph of $PSiO_2$ oxidized at 800 °C, focusing at the interface between the bulk Si support and porous layer. (c) Oxygen and (d) Si elemental mapping of the corresponding layer (blue and red, respectively).[37]

oxidation temperatures (400, 600, 800 °C). A significant increase in absorbance of the Si−O−Si stretching mode and the $-(O_ySiH_x)$ vibration mode (observed at 1039 and 801 cm^{-1}, respectively) with elevation of the oxidation temperature is shown in the Supporting Information, Figure S2a. These results correlate well with the disappearance of the $Si-H_x$ peak (observed at 878 cm^{-1}) at 600 and 800 °C, due to the oxidation of all hydrogen-terminated Si groups. Figure S2b in the Supporting Information shows a similar increase in the absorbance of the Si−OH vibration mode at 3747 cm^{-1}, resulting from a thicker oxide layer.[38]

Nitrogen adsorption−desorption experiments followed by BET and BJH analyses are used to further characterize the different oxidized PSi films, in terms of the pore size distribution, specific surface area, and porous volume. Table 1

Table 1. Physical Characteristics of PSi Films Oxidized at Different Temperatures (400, 600, 800°C) Measured by Nitrogen Adsorption−Desorption and Gravimetry

oxidn temp (°C)	av pore diam[a] (nm)	total porosity[b] (%)	surf. area[c] ($m^2\ g^{-1}$)	porous vol[c] ($cm^3\ g^{-1}$)
400	16.1	83 ± 1	268.8 ± 0.6	1.13 ± 0.02
600	15.8	80 ± 1	257.7 ± 1.0	1.08 ± 0.02
800	11.8	75 ± 1	247.7 ± 0.6	0.81 ± 0.02

[a]Values calculated from nitrogen desorption isotherms using the BJH model. [b]Measured by gravimetric analysis. [c]Values calculated based on the BET model.

summarizes the physical characteristics of the different oxidized films. The average pore diameter and the total porosity (obtained by gravimetric analysis) decrease with the increase of the oxidation temperature. The resulting pore clogging by the oxygen layer obtained at elevated temperatures lowers the porous volume and accordingly the surface area.[33] It should be noted that the pore diameter obtained by this method is significantly lower than the visual estimates by HRSEM (Table 1), as previously reported.[3]

Biofunctionalization of $PSiO_2$ with Enzymes. The synthetic approach for grafting enzymes onto the three different oxidized surfaces is based on a well-described silanization methodology.[39,40] First, APTES in combination with organic base DIEA are used to introduce amino groups to the thermally oxidized nanostructures and obtain an activated surface for grafting of the homobifunctional cross-linker DSC. The cross-linker reacts with primary amines through nucleophilic attack of the amine on the C═O succinimidyl ester, eliminating one NHS group. Finally, primary amines stemming from the surface Lys groups of the HRP enzyme are used for immobilization onto the surface via the second reactive group of the DSC,[39] as schematically illustrated in Figure 2. ATR-FTIR spectroscopy is

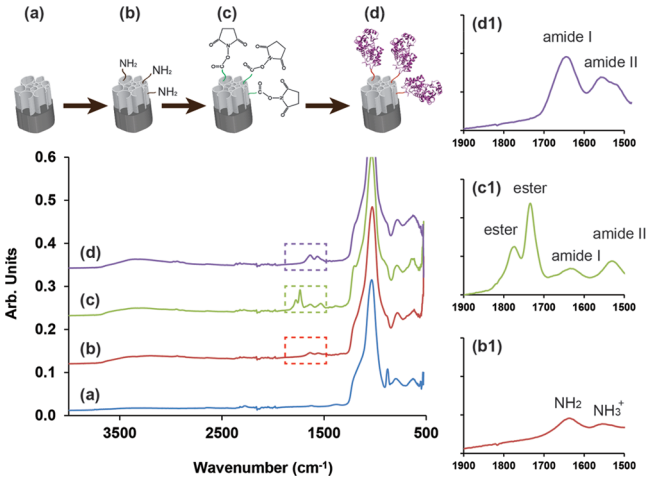

Figure 2. (top) Schematic illustration of synthetic steps followed for enzyme immobilization onto $PSiO_2$ surface: (a) neat $PSiO_2$ surface oxidized at 400 °C; (b) APTES-modified surface; (c) DSC-modified surface; (d) HRP-immobilized surface. (bottom) Corresponding ATR-FTIR spectra. (right) Insets b1, c1, and d1 show the corresponding spectra for clarity.

used to confirm the modification of the porous scaffold. The ATR-FTIR spectra of the different surfaces oxidized at 400 °C (neat $PSiO_2$, APTES, DSC, and HRP) are shown in Figure 2. The neat $PSiO_2$ surface spectrum (Figure 2, trace a) shows a typical $-(O_ySiH_x)$ vibration mode at 801 cm^{-1} and a peak at 1039 cm^{-1} that is related to the Si−O−Si stretching mode. The APTES-modified surface spectrum (Figure 2, traces b and b1) depicts two additional peaks; the 1641 cm^{-1} peak is ascribed to the bending of primary amine and the 1555 cm^{-1} peak is ascribed to the bending of protonated amines. The spectra taken following modification with DSC is displayed in Figure 2, traces c and c1. Amide bands appear at 1635 and 1531 cm^{-1} (amide I and amide II, respectively), exhibiting a red shift compared to bands of the APTES-modified surface. Moreover, two substantial peaks appearing at 1734 and 1774 cm^{-1} (Figure 2, trace c1) are ascribed to the asymmetric and symmetric stretching bands of succinimidyl ester, respectively.[39] Finally, for the HRP-immobilized surface (Figure 2, traces d and d1), amide bands appear at 1645 and 1558 cm^{-1} (amide I and amide II, respectively), showing a blue shift compared to the DSC-modified surface. These results verify that the HRP macromolecules are conjugated to the $PSiO_2$ surface. ATR-FTIR spectra for the biofunctionalization of the other two surfaces (oxidized at 600 and 800 °C) show identical spectra (data not shown).

Reflective Interferometric Fourier Transform Spectroscopy. To monitor the optical changes following different

biofunctionalization steps on the $PSiO_2$ surfaces, reflective interferometric Fourier transform spectroscopy (RIFTS) is used as an additional tool. This method is characterized by high sensitivity to minor alterations in the average refractive index of the porous nanostructure and thus allows for direct and real-time monitoring of the binding of different species onto the pore walls.[1,2,7−9,41] It is expected that chemical modification of the $PSiO_2$ surfaces (as illustrated in Figure 2) will induce a red shift in the EOT due to the increase in the value of n upon immobilization of the different biomolecules. It should be noted that the $PSiO_2$ nanostructure is designed to allow a proper infiltration of the desired biomolecules into the pores. Indeed, substantial relative EOT changes are perceived after each of the described immobilization steps for the three different oxidized surfaces (400, 600, and 800 °C); see Figure 3.

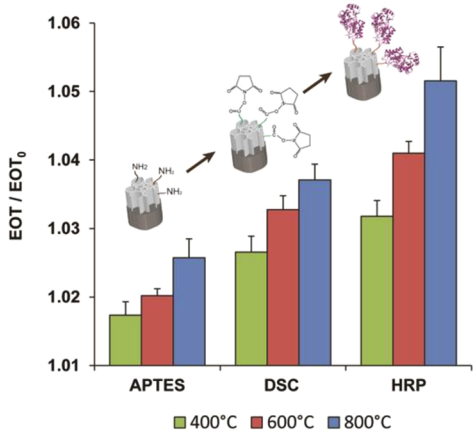

Figure 3. Relative EOT changes upon HRP biofunctionalization onto $PSiO_2$ scaffolds oxidized at different temperatures. The synthetic steps followed for enzyme immobilization onto the $PSiO_2$ surface are (i) APTES modification, (ii) DSC modification, and (iii) HRP conjugation. Note that the EOT values obtained after each modification step are normalized with respect to the EOT value of the neat oxidized PSi scaffold (termed as EOT_0) at a specific temperature.

Additionally, the EOT values after each modification are observed to increase, as the oxidation temperature rises (e.g., after silanization, increases of 1.017 ± 0.002, 1.020 ± 0.001, and 1.0257 ± 0.003 in the relative EOT or 245 ± 28, 285 ± 9, and 338 ± 54 nm shifts are observed for oxidation temperatures of 400, 600, and 800 °C, respectively). This phenomenon can be ascribed to the increase of the amount of Si−OH present on the surface at elevated temperatures (see Supporting Information, Figure S2, for details), which serves as an anchor for the following biofunctionalization steps.[29,30]

Quantification of Immobilized Enzyme. Two different classes of enzymes are investigated in this study. First, HRP, one of the most powerful peroxidases with a molecular weight of 44 kDa and dimensions of 6.2 × 4.3 × 1.2 nm^3 (Figure 4), is used.[42,43] The second is trypsin, an extensively used protease for peptide mapping, characterized by a molecular weight of 24 kDa and typical dimensions of 3.8 × 3.8 × 3.8 nm^3 (Figure 4).[44] To quantify the amount of enzymes anchored onto the different $PSiO_2$ scaffolds, the substrate oxidization capability of HRP and proteolytic activity of trypsin are studied using colorimetric tests. Enzyme-immobilized $PSiO_2$ surfaces are introduced with the corresponding substrates (Ampliflu Red and FTC-casein for HRP and trypsin, respectively) and allowed

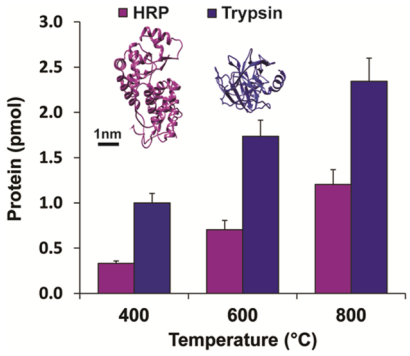

Figure 4. Quantification of immobilized enzymes (HRP and trypsin) onto $PSiO_2$ at three different oxidation temperatures (400, 600, 800 °C). (inset) Three-dimensional structure of immobilized enzymes analyzed by Chimera program.[49] Note that enzyme quantification is performed by comparing the specific activity of the immobilized enzyme to that of the unrestricted enzyme in a solution.

to react, while the specific activity parameters are spectrophotometrically evaluated. By comparing the obtained results to the respective activity values of the neat enzymes in solution, we estimate the amount of enzyme immobilized onto the different oxide layers;[35] see Figure 4. For both HRP and trypsin, a clear trend of a higher immobilized enzyme amount is obtained as the oxidation temperature is raised: values as high as 1.2 ± 0.2 and 2.3 ± 0.3 pmol at 800 °C are calculated for HRP and trypsin, respectively. These results are in agreement with the RIFTS experiments results, presented in the section Reflective Interferometric Fourier Transform Spectroscopy. It should be noted that the quantification of the enzymes is performed by comparing the specific activity of the immobilized enzymes to that of the free enzymes in a solution, assuming that all immobilized enzymes are fully active.[35,45] This assumption underestimates the extent of enzyme immobilization as it does not consider important parameters such as enzyme−support interactions, diffusion limits, structural changes in the enzyme induced by the local surface geometry, and nanoconfinement effects. All these parameters may impair the catalytic performances of immobilized enzyme.[46,47] The obtained results agree well with steric crowding effects, which significantly affect the immobilization efficiency of biomolecules onto the porous scaffold.[14,25,48] Thus, as the gyration radius of trypsin is smaller than that of HRP (approximately 2-fold smaller), its physical accessibility into the porous nanostructure is expected to be higher, resulting in a greater immobilization efficiency. Indeed, significantly higher values (>2 times) of immobilized trypsin are observed at all oxidation conditions, as shown in Figure 4. Moreover, these results show that, despite the decrease in porous volume upon thermal oxidation at elevated temperatures (Table 1), the pore clogging by a thicker oxide layer has no negative effect on enzyme immobilization. On the contrary, the substantial oxide layer offers the means for effective surface coverage and successful biofunctionalization (e.g., higher coverage of Si−OH groups at elevated temperatures).

To further characterize the extent of the enzyme immobilization within the different $PSiO_2$ scaffolds, fluorescein-labeled HRP (FTC-HRP) and trypsin are immobilized as previously discussed, followed by observation using a confocal laser scanning microscope (CLSM). Figure 5 presents CLSM 3D projection images of $PSiO_2$ nanostructures following the immobilization of (FTC-HRP). The fluorescence intensity is observed to significantly increase with oxidation temperature

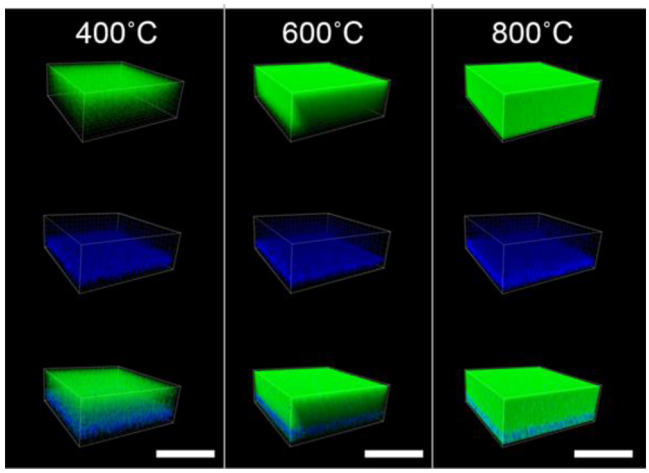

Figure 5. CLSM 3D projection images of fluorescently labeled HRP immobilized onto $PSiO_2$ nanostructures oxidized at three temperatures (400, 600, 800 °C). (top) FTC-HRP immobilized surfaces. (middle) Photoluminescence (PL) of different oxidized porous scaffolds. (bottom) Combined view of top and middle rows. The scale bar is 10 μm.

(see Figure 5, top-row images), indicative of higher enzyme immobilization efficiency. The fluorescence signal from the labeled HRP is observed throughout the entire volume of the porous scaffold, for $PSiO_2$ processed at higher temperatures; see Figure S3 in the Supporting Information for details. A similar trend is obtained when FTC-trypsin is immobilized onto the different $PSiO_2$ layers (data not shown). Figure 5 (middle row) and Figure S3 in the Supporting Information depict the photoluminescence (PL) of the $PSiO_2$ skeleton. The PL intensity increases as the oxide layer is grown at elevated temperatures.[33,50−53] These results further confirm that the thicker and more uniform oxide layer, obtained at elevated temperatures, has a profound impact on the extent of enzyme immobilization.[33] This is clearly observed in Figure 5 (bottom row), which combines the PL (originating from the $PSiO_2$ scaffold) and the fluorescence (from the labeled HRP) signals, where the labeled enzyme densely decorates the porous scaffold throughout.

Optical Signal Stability in Aqueous Media. Before we investigate the potential of the enzyme-immobilized $PSiO_2$ platforms to act as an optical biosensor for label-free monitoring of enzyme activity, their optical readout stability in biologically relevant media should be assessed.[4,10,25,35,39] Thus, two transducers (neat $PSiO_2$ and enzyme-immobilized $PSiO_2$) are fixed in a flow cell and HEPES buffer is circulated, while their optical properties are monitored in real time. Figure 6 depicts the changes in the relative EOT as a function of time for neat $PSiO_2$ and the corresponding HRP-immobilized $PSiO_2$ layers. During 4 h buffer flow experiments, negligible baseline drift in EOT values (4.0×10^{-7} min^{-1}, see Figure S4 in the Supporting Information) is observed for HRP-immobilized $PSiO_2$, which is oxidized at 800 °C. On the contrary, HRP-immobilized $PSiO_2$ films oxidized at lower temperatures of 400 and 600 °C show a significant and rapid decrease in their relative EOT values (9.0×10^{-6} and 2.9×10^{-6} min^{-1}, respectively; see Figure S4 in the Supporting Information). These profound changes in the EOT signals are attributed to time-dependent degradation and dissolution of the porous scaffold.[4,25,27] A similar trend is observed for neat $PSiO_2$ (no enzyme), APTES-modified $PSiO_2$, DSC-modified $PSiO_2$, and

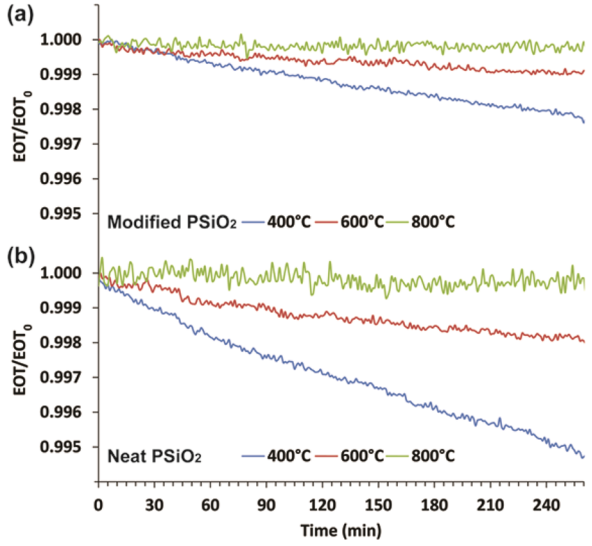

Figure 6. Optical response, expressed in terms of relative EOT, of enzyme-immobilized and neat $PSiO_2$ films vs exposure time to aqueous solution flow conditions. The nanostructures are continuously washed with HEPES buffer at 0.5 mL min^{-1}. (a) HRP-immobilized $PSiO_2$ oxidized at three different temperatures (400, 600, 800 °C). (b) Neat $PSiO_2$ (no enzyme) oxidized under similar conditions.

trypsin-immobilized $PSiO_2$ films, shown in Figure 6b and Figures S5, S6, and S7, respectively, in the Supporting Information. Thus, these results clearly demonstrate that the optical readout of the neat $PSiO_2$, APTES-modified $PSiO_2$, DSC-modified $PSiO_2$, and enzyme-immobilized $PSiO_2$ are highly stable at elevated temperatures (800 °C) under biologically relevant aqueous conditions. It should be noted the surface modification and the enzyme immobilization process facilitate the optical signal stability at lower oxidation temperatures due to surface passivation (Supporting Information, Figure S4).

Optical Monitoring of Enzymatic Activity. Previous sections have confirmed that the oxidation temperature of the porous nanostructure has a profound effect on the enzyme immobilization efficiency and the optical signal stability. Next, we investigate the potential of HRP-immobilized $PSiO_2$ scaffolds to serve as an optical biosensor for monitoring sensitive biochemical reactions through RIFTS experiments and the influence of the oxide layer on the biosensor's performance. Figure 7 shows the relative EOT change of HRP-immobilized $PSiO_2$ after introduction of the substrate, 4-chloro-1-naphthol (4CN), which is oxidized by HRP into an insoluble product, 4-chloro-1-naphthon (4CNn).[36,54] A rapid increase in the relative EOT values is observed after addition of 0.16 M H_2O_2 to the cycled solution for all oxidized surfaces (Figure 7II). This increase is ascribed to the precipitation and accumulation of the enzymatic reaction product within the pores,[55] as schematically illustrated in Figure 7. As the oxidation temperature is increased from 400 to 800 °C, more significant EOT changes rapidly introduced to the system are observed. This can be attributed to the higher enzyme content within the different $PSiO_2$ scaffolds, which results in the higher substrate oxidation efficiency and rapid pore blockage by insoluble product.

■ CONCLUSIONS

We demonstrate the effect of the oxidation temperature on the chemical stability of $PSiO_2$ optical transducers. A substantial

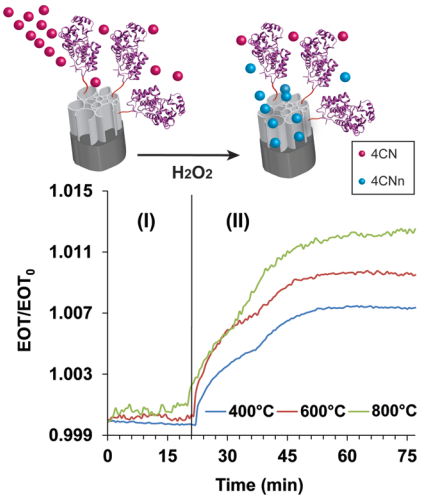

Figure 7. Schematic illustration of optical response of HRP-immobilized $PSiO_2$ to enzymatic reaction products infiltrating the nanostructure (red dots, 4CN; blue dots, 4CNn). HRP-immobilized $PSiO_2$ (oxidized at 400, 600, 800 °C) is pretreated with HEPES buffer to reduce nonspecific adsorption of enzymes. (I) Wash with 0.8 mM 4CN in HEPES buffer (pH 8). (II) Introduction of 0.16 M H_2O_2 to the cycled solution.

oxide layer formed at different temperatures stabilizes the highly porous scaffold and thus preserves the characteristic optical properties in biologically relevant media. Importantly, by monitoring the catalytic activity of HRP-immobilized $PSiO_2$, we show that the thermal oxidation profoundly affects the biosensing performance in terms of greater optical sensitivity. Thus, despite the significant decrease in specific surface area upon thermal oxidation at elevated temperatures, higher enzyme content and surface coverage are achieved, leading to enhancement of the biosensor's sensitivity. Therefore, surface passivation by thermal oxidation enhances the PSi versatility and applicability as a fundamental platform for the development of optical sensing systems.

■ ASSOCIATED CONTENT

Supporting Information

Results of TGA, ATR-FTIR, image analysis, and optical stability experiments. This material is available free of charge via the Internet at http://pubs.acs.org.

■ AUTHOR INFORMATION

Corresponding Author

*E-mail: esegal@tx.technion.ac.il. Tel.: +972-4-8295071. Fax: +972-4-8293399.

Author Contributions

The manuscript was written through contributions of all authors. All authors have given approval to the final version of the manuscript.

Notes

The authors declare no competing financial interest.

■ ACKNOWLEDGMENTS

E.S. acknowledges the financial support of the Russell Berrie Nanotechnology Institute (RBNI) and the Lorry I. Lokey Center for Life Science and Engineering. G.S. is most grateful for the Russell Berrie Scholarships for Outstanding Graduate Students.

■ REFERENCES

(1) Jane, A.; Dronov, R.; Hodges, A.; Voelcker, N. H. Porous Silicon Biosensors on the Advance. *Trends Biotechnol.* **2009**, *27*, 230−239.
(2) Sailor, M. J.; Link, J. R. "Smart Dust": Nanostructured Devices in a Grain of Sand. *Chem. Commun.* **2005**, 1375−1383.
(3) Segal, E.; Perelman, L. A.; Cunin, F.; Di Renzo, F.; Devoisselle, J.-M.; Li, Y. Y.; Sailor, M. J. Confinement of Thermoresponsive Hydrogels in Nanostructured Porous Silicon Dioxide Templates. *Adv. Funct. Mater.* **2007**, *17*, 1153−1162.
(4) Massad-Ivanir, N.; Shtenberg, G.; Segal, E. Advancing Nanostructured Porous Si-Based Optical Transducers for Label Free Bacteria Detection. *Adv. Exp. Med. Biol.* **2012**, *733*, 37−45.
(5) Kilian, K. A.; Lai, L. M. H.; Magenau, A.; Cartland, S.; Böcking, T.; Di Girolamo, N.; Gal, M.; Gaus, K.; Gooding, J. J. Smart Tissue Culture: In Situ Monitoring of the Activity of Protease Enzymes Secreted from Live Cells Using Nanostructured Photonic Crystals. *Nano Lett.* **2009**, *9*, 2021−2025.
(6) Massad-Ivanir, N.; Shtenberg, G.; Tzur, A.; Krepker, M. A.; Segal, E. Engineering Nanostructured Porous SiO2 Surfaces for Bacteria Detection Via "Direct Cell Capture". *Anal. Chem.* **2011**, *83*, 3282−3289.
(7) Kilian, K. A.; Boecking, T.; Gaus, K.; Gal, M.; Gooding, J. J. Peptide-Modified Optical Filters for Detecting Protease Activity. *ACS Nano* **2007**, *1*, 355−361.
(8) Pacholski, C.; Sartor, M.; Sailor, M. J.; Cunin, F.; Miskelly, G. M. Biosensing Using Porous Silicon Double-Layer Interferometers: Reflective Interferometric Fourier Transform Spectroscopy. *J. Am. Chem. Soc.* **2005**, *127*, 11636−11645.
(9) Orosco, M. M.; Pacholski, C.; Sailor, M. J. Real-Time Monitoring of Enzyme Activity in a Mesoporous Silicon Double Layer. *Nat. Nanotechnol.* **2009**, *4*, 255−258.
(10) Bonanno, L. M.; Segal, E. Nanostructured Porous Silicon-Polymer-Based Hybrids: From Biosensing to Drug Delivery. *Nanomedicine* **2011**, *6*, 1755−1770.
(11) Pace, S.; Seantier, B.; Belamie, E.; Lautredou, N.; Sailor, M. J.; Milhiet, P.-E.; Cunin, F. Characterization of Phospholipid Bilayer Formation on a Thin Film of Porous SiO2 by Reflective Interferometric Fourier Transform Spectroscopy (RIFTS). *Langmuir* **2012**, *28*, 6960−6969.
(12) Bonanno, L. M.; DeLouise, L. A. Tunable Detection Sensitivity of Opiates in Urine Via a Label-Free Porous Silicon Competitive Inhibition Immunosensor. *Anal. Chem.* **2010**, *82*, 714−722.
(13) Guan, B.; Ciampi, S.; Le Saux, G.; Gaus, K.; Reece, P. J.; Gooding, J. J. Different Functionalization of the Internal and External Surfaces in Mesoporous Materials for Biosensing Applications Using "Click" Chemistry. *Langmuir* **2011**, *27*, 328−334.
(14) Kilian, K. A.; Boecking, T.; Gooding, J. J. The Importance of Surface Chemistry in Mesoporous Materials: Lessons from Porous Silicon Biosensors. *Chem. Commun.* **2009**, 630−640.
(15) Miller, B. L. Nano-structured Silicon Optical Sensors. In *Optical Guided-Wave Chemical and Biosensors II*; Zourob, M., Lakhtakia, A., Eds.; Springer Series on Chemical Sensors and Biosensors 8; Springer: Berlin, 2010; pp 3−25.
(16) Pal, S.; Guillermain, E.; Sriram, R.; Miller, B. L.; Fauchet, P. M. Silicon Photonic Crystal Nanocavity-Coupled Waveguides for Error-Corrected Optical Biosensing. *Biosens. Bioelectron.* **2011**, *26*, 4024−4031.
(17) Rong, G.; Najmaie, A.; Sipe, J. E.; Weiss, S. M. Nanoscale Porous Silicon Waveguide for Label-Free DNA Sensing. *Biosens. Bioelectron.* **2008**, *23*, 1572−1576.
(18) Szili, E. J.; Jane, A.; Low, S. P.; Sweetman, M.; Macardle, P.; Kumar, S.; Smart, R. S. C.; Voelcker, N. H. Interferometric Porous Silicon Transducers Using an Enzymatically Amplified Optical Signal. *Sens. Actuators, B* **2011**, *160*, 341−348.
(19) Qiao, H.; Guan, B.; Gooding, J. J.; Reece, P. J. Protease Detection Using a Porous Silicon Based Bloch Surface Wave Optical Biosensor. *Opt. Express* **2010**, *18*, 15174−15182.
(20) Pacholski, C. Photonic Crystal Sensors Based on Porous Silicon. *Sensors* **2013**, *13*, 4694−4713.

(21) Voelcker, N. H.; Alfonso, I.; Ghadiri, M. R. Catalyzed Oxidative Corrosion of Porous Silicon Used as an Optical Transducer for Ligand−Receptor Interactions. *ChemBioChem* **2008**, *9*, 1776−1786.
(22) Freedman, K. J.; Bastian, A. R.; Chaiken, I.; Kim, M. J. Solid-State Nanopore Detection of Protein Complexes: Applications in Healthcare and Protein Kinetics. *Small* **2013**, *9*, 750−759.
(23) Secret, E.; Maynadier, M.; Gallud, A.; Gary-Bobo, M.; Chaix, A.; Belamie, E.; Maillard, P.; Sailor, M. J.; Garcia, M.; Durand, J.-O.; Cunin, F. Anionic Porphyrin-Grafted Porous Silicon Nanoparticles for Photodynamic Therapy. *Chem. Commun.* **2013**, *49*, 4202−4204.
(24) Libertino, S.; Giannazzo, F.; Aiello, V.; Scandurra, A.; Sinatra, F.; Renis, M.; Fichera, M. XPS and AFM Characterization of the Enzyme Glucose Oxidase Immobilized on SiO2 Surfaces. *Langmuir* **2008**, *24*, 1965−1972.
(25) Tsang, C. K.; Kelly, T. L.; Sailor, M. J.; Li, Y. Y. Highly Stable Porous Silicon−Carbon Composites as Label-Free Optical Biosensors. *ACS Nano* **2012**, *6*, 10546−10554.
(26) Gupta, B.; Zhu, Y.; Guan, B.; Reece, P. J.; Gooding, J. J. Functionalised Porous Silicon as a Biosensor: Emphasis on Monitoring Cells in Vivo and in Vitro. *Analyst* **2013**, *138*, 3593−3615.
(27) Janshoff, A.; Dancil, K. P. S.; Steinem, C.; Greiner, D. P.; Lin, V. S. Y.; Gurtner, C.; Motesharei, K.; Sailor, M. J.; Ghadiri, M. R. Macroporous P-Type Silicon Fabry-Perot Layers. Fabrication, Characterization, and Applications in Biosensing. *J. Am. Chem. Soc.* **1998**, *120*, 12108−12116.
(28) Libertino, S.; Scandurra, A.; Aiello, V.; Giannazzo, F.; Sinatra, F.; Renis, M.; Fichera, M. Layer Uniformity in Glucose Oxidase Immobilization on SiO2 Surfaces. *Appl. Surf. Sci.* **2007**, *253*, 9116−9123.
(29) Pap, A. E.; Kordas, K.; George, T. F.; Leppavuori, S. Thermal Oxidation of Porous Silicon: Study on Reaction Kinetics. *J. Phys. Chem. B* **2004**, *108*, 12744−12747.
(30) Cisneros, R.; Pfeiffer, H.; Wang, C. Oxygen Absorption in Free-Standing Porous Silicon: A Structural, Optical and Kinetic Analysis. *Nanoscale Res. Lett.* **2010**, *5*, 686−691.
(31) Jarvis, K. L.; Barnes, T. J.; Prestidge, C. A. Thermal Oxidation for Controlling Protein Interactions with Porous Silicon. *Langmuir* **2010**, *26*, 14316−14322.
(32) De Stefano, L.; Oliviero, G.; Amato, J.; Borbone, N.; Piccialli, G.; Mayol, L.; Rendina, I.; Terracciano, M.; Rea, I. Aminosilane Functionalizations of Mesoporous Oxidized Silicon for Oligonucleotide Synthesis and Detection. *J. R. Soc., Interface* **2013**, *10*, 1−7.
(33) Salonen, J.; Mäkilä, E. In *Porous Silicon for Biomedical Applications*; Santos, H. A., Ed.; Woodhead Publishing Ltd.: Cambridge, U.K., 2014; Chapter 2, pp 21−34.
(34) Tzur-Balter, A.; Rubinski, A.; Segal, E. Designing Porous Silicon-Based Microparticles as Carriers for Controlled Delivery of Mitoxantrone Dihydrochloride. *J. Mater. Res.* **2013**, *28*, 231−239.
(35) Shtenberg, G.; Massad-Ivanir, N.; Moscovitz, O.; Engin, S.; Sharon, M.; Fruk, L.; Segal, E. Picking up the Pieces: A Generic Porous Si Biosensor for Probing the Proteolytic Products of Enzymes. *Anal. Chem.* **2013**, *85*, 1951−1956.
(36) Shtenberg, G.; Massad-Ivanir, N.; Engin, S.; Sharon, M.; Fruk, L.; Segal, E. DNA-Directed Immobilization of Horseradish Peroxidase onto Porous SiO2 Optical Transducers. *Nanoscale Res. Lett.* **2012**, *7*, 1−6.
(37) Shtenberg, G.; Massad-Ivanir, N.; Fruk, L.; Segal, E. Effect of Thermal Oxidation on the Performance of Nanostructured Porous Si Optical Biosensors. Presented at the Porous Semiconductors—Science and Technology (PSST) Conference, Benidorm, Spain; March 9−14, 2014.
(38) Mawhinney, D. B.; Glass, J. A.; Yates, J. T. FTIR Study of the Oxidation of Porous Silicon. *J. Phys. Chem. B* **1997**, *101*, 1202−1206.
(39) Xia, B.; Xiao, S. J.; Guo, D. J.; Wang, J.; Chao, M.; Liu, H. B.; Pei, J.; Chen, Y. Q.; Tang, Y. C.; Liu, J. N. Biofunctionalisation of Porous Silicon (Ps) Surfaces by Using Homobifunctional Cross-Linkers. *J. Mater. Chem.* **2006**, *16*, 570−578.
(40) Subramanian, A.; Kennel, S. J.; Oden, P. I.; Jacobson, K. B.; Woodward, J.; Doktycz, M. J. Comparison of Techniques for Enzyme Immobilization on Silicon Supports. *Enzyme Microb. Technol.* **1999**, *24*, 26−34.
(41) Sailor, M. J. *Porous Silicon in Practice: Preparation, Characterization and Applications*, 1st ed.; Wiley-VCH: Weinheim, Germany, 2012.
(42) Zhang, J. D.; Chi, Q. J.; Dong, S. J.; Wang, E. K. In Situ Electrochemical Scanning Tunnelling Microscopy Investigation of Structure for Horseradish Peroxidase and Its Electrocatalytic Property. *Bioelectrochem. Bioenerg.* **1996**, *39*, 267−274.
(43) Loew, N.; Bogdanoff, P.; Herrmann, I.; Wollenberger, U.; Scheller, F. W.; Katterle, M. Influence of Modifications on the Efficiency of Pyrolysed CoTMPP as Electrode Material for Horseradish Peroxidase and the Reduction of Hydrogen Peroxide. *Electroanalysis* **2006**, *18*, 2324−2330.
(44) Min, Q.; Wu, R. A.; Zhao, L.; Qin, H.; Ye, M.; Zhu, J.-J.; Zou, H. Size-Selective Proteolysis on Mesoporous Silica-Based Trypsin Nanoreactor for Low-Mw Proteome Analysis. *Chem. Commun.* **2010**, *46*, 6144−6146.
(45) Fang, S.-M.; Wang, H.-N.; Zhao, Z.-X.; Wang, W.-H. Immobilized Enzyme Reactors in HPLC and Its Application in Inhibitor Screening: A Review. *J. Pharm. Anal.* **2012**, *2*, 83−89.
(46) Zhang, F.; Wang, M.; Liang, C.; Jiang, H.; Shen, J.; Li, H. Thin-Layer Polymer Wrapped Enzymes Encapsulated in Hierarchically Mesoporous Silica with High Activity and Enhanced Stability. *Sci. Rep.* **2014**, *4*, 4421−4421.
(47) Lei, C.; Shin, Y.; Liu, J.; Ackerman, E. J. Entrapping Enzyme in a Functionalized Nanoporous Support. *J. Am. Chem. Soc.* **2002**, *124*, 11242−11243.
(48) Bonanno, L. M.; DeLouise, L. A. Steric Crowding Effects on Target Detection in an Affinity Biosensor. *Langmuir* **2007**, *23*, 5817−5823.
(49) Pettersen, E. F.; Goddard, T. D.; Huang, C. C.; Couch, G. S.; Greenblatt, D. M.; Meng, E. C.; Ferrin, T. E. UCSF Chimera—a Visualization System for Exploratory Research and Analysis. *J. Comput. Chem.* **2004**, *25*, 1605−1612.
(50) Cullis, A. G.; Canham, L. T.; Calcott, P. D. J. The Structural and Luminescence Properties of Porous Silicon. *J. Appl. Phys.* **1997**, *82*, 909−965.
(51) Kontkiewicz, A. J.; Kontkiewicz, A. M.; Siejka, J.; Sen, S.; Nowak, G.; Hoff, A. M.; Sakthivel, P.; Ahmed, K.; Mukherjee, P.; Witanachchi, S.; Lagowski, J. Evidence That Blue Luminescence of Oxidized Porous Silicon Originates from SiO2. *Appl. Phys. Lett.* **1994**, *65*, 1436−1438.
(52) Sailor, M. J.; Wu, E. C. Photoluminescence-Based Sensing with Porous Silicon Films, Microparticles, and Nanoparticles. *Adv. Funct. Mater.* **2009**, *19*, 3195−3208.
(53) Saar, A. Photoluminescence from Silicon Nanostructures: The Mutual Role of Quantum Confinement and Surface Chemistry. *J. Nanophotonics* **2009**, *3*, 032501−032542.
(54) Kumada, Y.; Maehara, M.; Tomioka, K.; Katoh, S. Liposome Immunoblotting Assay Using a Substrate-Forming Precipitate inside Immunoliposomes. *Biotechnol. Bioeng.* **2002**, *80*, 414−418.
(55) Fortin, E.; Mailley, P.; Lacroix, L.; Szunerits, S. Imaging of DNA Hybridization on Microscopic Polypyrrole Patterns Using Scanning Electrochemical Microscopy (SECM): The HRP Bio-Catalyzed Oxidation of 4-Chloro-1-Naphthol. *Analyst* **2006**, *131*, 186−193.